Chapter 9

PID Controller Design Methods for Multi-Mass Resonance System

Hidehiro Ikeda

Additional information is available at the end of the chapter

http://dx.doi.org/10.5772/intechopen.74298

Abstract

Motor drive systems are indispensable for applications in the industrial field. High-speed and high-accuracy control is required for motor drive systems. However, solutions to meet these requirements can cause mechanical resonance vibrations to occur in the system as a result of miniaturization and system weight reduction. It is therefore necessary to model these systems as multi-mass resonance systems with multiple masses and finite rigid shafts, gears, and loads. In addition, vibration suppression control should be applied to these systems. This chapter provides two off-line tuning methods for a digital proportional-integral-derivative (PID)-type controller for a two-mass resonance system to suppress its mechanical resonance vibrations. These methods include a coefficient diagram method and a fictitious reference iterative tuning method. The former method uses a nominal mathematical model of the object while the latter method uses only the initial experimental data without use of the mathematical model. In this chapter, the two methods are compared. A controller is proposed that consists of a modified integral-proportional derivative (I-PD) speed controller and a proportional-integral (PI) current controller, and requires no information about the load side state variables. Finally, the effectiveness of the proposed method is confirmed through computer simulations and experimental results.

Keywords: two-mass resonance system, vibration suppression control, modified I-PD controller, coefficient diagram method, fictitious reference iterative tuning

1. Introduction

Motor drive systems are used in a wide range of applications, including industrial robots, home electrical appliances, automobiles, steel rolling mills, computers, and space work surfaces. In

general, motor drive systems consist of electric motors, gears, belts, flexible shafts, and mechanical load equipment. Recently, the overall stiffness of these systems has been decreasing because of demands for high-speed and high-accuracy system responses, miniaturization, system weight reduction, and low system costs. Additionally, the system constructions have become more complex and the central processing unit (CPU) processing speeds that are required to perform the system calculations have increased exponentially. Consequently, torsional resonance vibrations occur between the motor and the load side. It is therefore necessary to model the system as a multi-mass resonance system, which is composed of several masses with finite rigid shafts, gears, and loads. In addition, a vibration suppression control method should be applied to the system.

The first-order approximation model of the multi-mass resonance system has the form of a two-mass resonance model. Several control methods are effective for control of a two-mass resonance system [1–5]. PID-type controllers are the most commonly used controllers for industrial applications because of their simplicity and their practicality for use with multi-mass systems. Various PID controller design methods have been proposed; examples of these methods include the limit sensitivity method, the Ziegler and Nichols tuning method, and methods that use the system polynomial. These controller design methods, which are called model-based design methods, may be able to produce the required results in cases where both the system equation and the real system's parameters are unknown.

In the industrial fields in which many typical motor drive systems are used, experienced technicians often adjust the control system on site to suit the needs of the manufacturing equipment. However, engineer shortages in these fields are becoming a serious problem. It is therefore essential to develop a simple controller design method for industrial applications.

Under these circumstances, and to save both the time required and the cost of tuning the controllers for the motor drive systems, some direct controller tuning methods have been proposed based on the transient response data from closed-loop systems, without modeling of the plant. The fictitious reference iterative tuning (FRIT) method is one of the most promising candidate methods for practical direct parameter tuning [6, 7]. Using the FRIT method, the controller gains can be designed using only single-shot experimental input-output data without knowledge of the model parameters of the object to be controlled.

This chapter introduces two types of approaches to PID-type controller design for suppression of the two-mass resonance system. The first method is based on the assumption that the mathematical model of the object to be controlled is known. This design method is called the coefficient diagram method (CDM) [8–10]. The CDM is an algebraic approach designed to produce the characteristic polynomial directly in the parameter space. The design of the coefficient diagram of the control system is performed using a differential evolution (DE) procedure to obtain the optimal controller gains in a short time [11–13]. The second design method is a FRIT method, which is a PID controller design approach based on one-shot experimental data only and does not use the mathematical model of the object to be controlled [14–16]. The effectiveness of the two proposed design methods is confirmed using a combination of computer simulations and experiments.

http://dx.doi.org/10.5772/intechopen.74298

2. Two-mass speed control system applying PID-type control

2.1. Description of two-mass resonance model

The model consists of two rigid masses and a torsional shaft. The multiple masses on the load side of the actual system are approximated as one inertial element. Similarly, several shafts and gears are approximated as a single torsional shaft. The typical two-mass model is depicted schematically in **Figure 1** below [14–17].

Here, J and ω denote the moment of inertia and the angular speed, respectively, and the suffixes M and L indicate the motor side and the load side, respectively. T_{in} is the input torque, T_{dis} is the torsional torque, T_L is the load torque, and K_s is the shaft stiffness. The continuous state equations of this two-mass resonance model are shown as Eqs. (1) to (3). Additionally, a current loop is considered in this research for high-speed torque control. Eq. (4) is indicative of the voltage equation when using a permanent magnet dc servo motor as the driving motor. In the equations, K_t is the torque constant of the dc motor, L_a is the armature current, R_a is the total resistance, u_c is the control input, K_e is the back-electromotive force (back-EMF) constant, and the viscous friction and nonlinear friction sources such as the Coulomb torque are neglected. Therefore, the torque input is calculated using $T_{in} = K_t i_a$.

$$J_M \frac{d\omega_M}{dt} = K_t i_a - T_{dis} \tag{1}$$

$$J_L \frac{d\omega_L}{dt} = T_{dis} - T_L \tag{2}$$

$$\frac{\mathrm{dT_{dis}}}{\mathrm{dt}} = \mathrm{K_s}(\omega_\mathrm{M} - \omega_\mathrm{L}) \tag{3}$$

$$L_a \frac{di_a}{dt} + R_a i_a = E u_c - K_e \omega_M \tag{4}$$

The research in this case deals with a normalized model to provide generality for the design of the proposed control system. Eqs. (5)–(8) show the normalized state equations. The state equation parameters are normalized as shown in Eq. (9), where the suffix *pu* indicates a normalized parameter, K_0 [V/pu] is the converter gain, K_a [pu/A] is the current feedback coefficient, K_ω [pu/(rad/s)] is the angular speed feedback gain, and τ_e [s] is an electrical time constant.

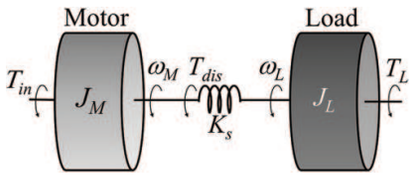

Figure 1. Two-mass resonance model.

$$J_{Mpu}\frac{d\omega_M}{dt} = i_a - T_{dis} \tag{5}$$

$$J_{Lpu}\frac{d\omega_L}{dt} = T_{dis} - T_L \tag{6}$$

$$\frac{dT_{dis}}{dt} = K_{spu}(\omega_M - \omega_L) \tag{7}$$

$$\tau_e\frac{di_a}{dt} + i_a = u_c - K_{epu}\omega_M \tag{8}$$

$$J_{Mpu} = \frac{K_a}{K_t K_\omega}J_M,\quad J_{Lpu} = \frac{K_a}{K_t K_\omega}J_L,\quad K_{spu} = \frac{K_a}{K_t K_\omega}K_s,\quad K_{epu} = \frac{1}{K_0 K_\omega}K_e \tag{9}$$

Therefore, the unit for all state variables is [pu]. **Figure 2** shows a block diagram of the normalized two-mass resonance model.

Eq. (10) gives the resonance angular frequency, the anti-resonance angular frequency, and the inertia ratio, respectively.

$$\omega_r = \sqrt{\frac{K_{spu}}{J_{Mpu}} + \frac{K_{spu}}{J_{Lpu}}},\quad \omega_a = \sqrt{\frac{K_{spu}}{J_{Lpu}}},\quad R = \frac{J_{Lpu}}{J_{Mpu}} \tag{10}$$

The next equation gives the simplified transfer function for the two-mass mechanical element, in which the input and the output are i_a and ω_M, respectively.

$$\frac{\Omega_M(s)}{I_a(s)} = \frac{s^2 + \omega_a^2}{J_{Mpu}s\left(s^2 + \omega_r^2\right)} \tag{11}$$

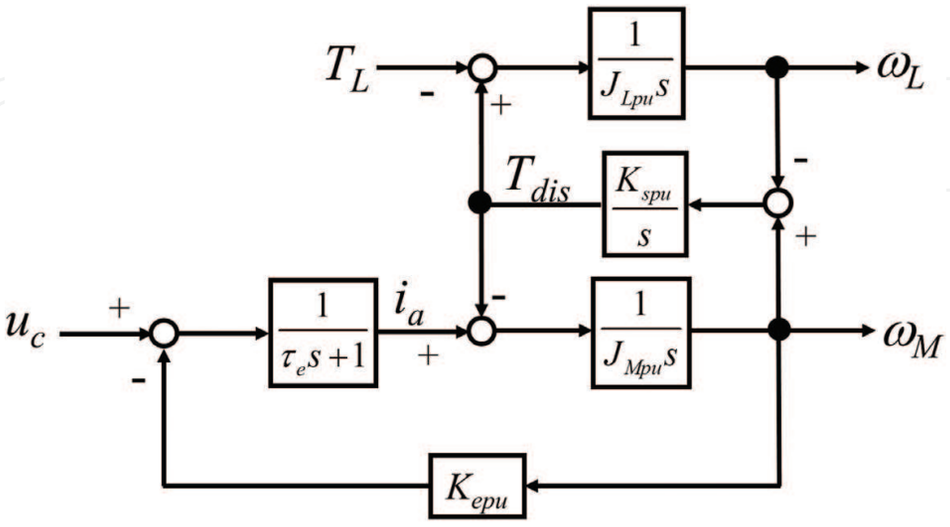

Figure 2. Block diagram of normalized two-mass resonance model.

http://dx.doi.org/10.5772/intechopen.74298

Symbol	Value	Symbol	Value
J_M	2.744×10^{-4} (kgm^2)	J_L	2.940×10^{-4} (kgm^2)
K_s	18.5 (Nm/rad)	R_a	2.884 (Ω)
L_a	6.676 (mH)	E	25.0 (V)
K_t	0.2778 (Nm/A)	K_e	0.2778 (V/(rad sec))

Table 1. Nominal parameters of the two-mass resonance model.

The nominal parameters for the two-mass resonance model in this chapter are given in **Table 1** below. In this chapter, the proposed CDM method is evaluated through computer simulations, while the proposed FRIT method is evaluated experimentally using the experimental setup shown below.

Figure 3 shows a photograph of the experimental system that was constructed in this research. The two-mass resonance system is simulated using the dc servo motor and a dc generator with a finite rigid coupling. The controller is realized using a digital signal processor that calculates the pulse-width modulation (PWM) signal to send to a four-quadrant dc chopper [17].

The digital signal processor (DSP) board (PE-PRO/F28335 Starter Kit, Myway Plus Corp.), consists of the DSP (TMS320F28335PGFA), a digital input/output (I/O), ABZ counters for the encoder signals, analogue-to-digital (A/D) converters and digital-to-analogue (D/A) converters [18]. The motor and load angles and the angular speeds are detected using 5000 pulses-per-revolution encoders. The dc servo motor current is measured using a current sensor and the A/D converter.

The control period (T_s) and the detection period of the encoder are both 1 ms and the current detection period is 10 μs. While we considered the application of the system to specific apparatus, we then constructed a digital control system that contains a discrete controller. In addition, we used MATLAB/Simulink software to perform the proposed off-line tuning process based on simulations and constructed the PID-type control system as a continuous system [19]. A disturbance is added to the dc generator as a torque using the electric load device on constant current mode. **Figure 4** shows the apparatus for the two-mass resonance model that was used in the experimental setup. **Figure 5** shows the experimental system configuration [17].

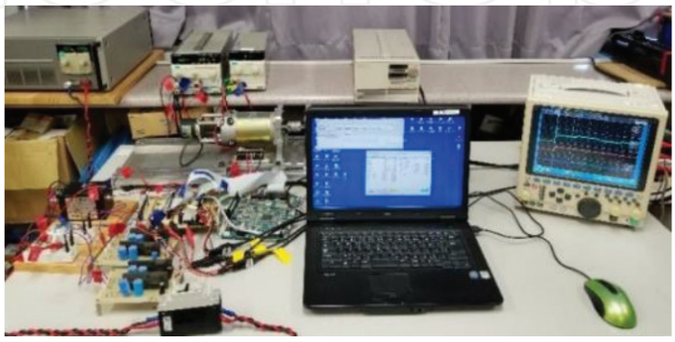

Figure 3. Overview of the experimental system.

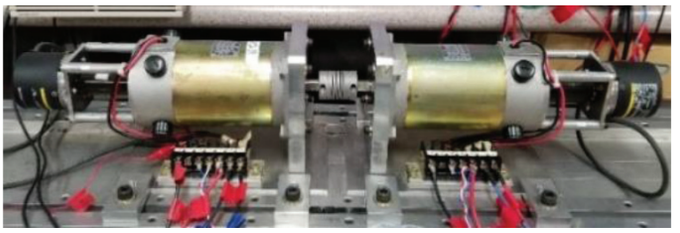

Figure 4. Photograph of the experimental two-mass resonance model.

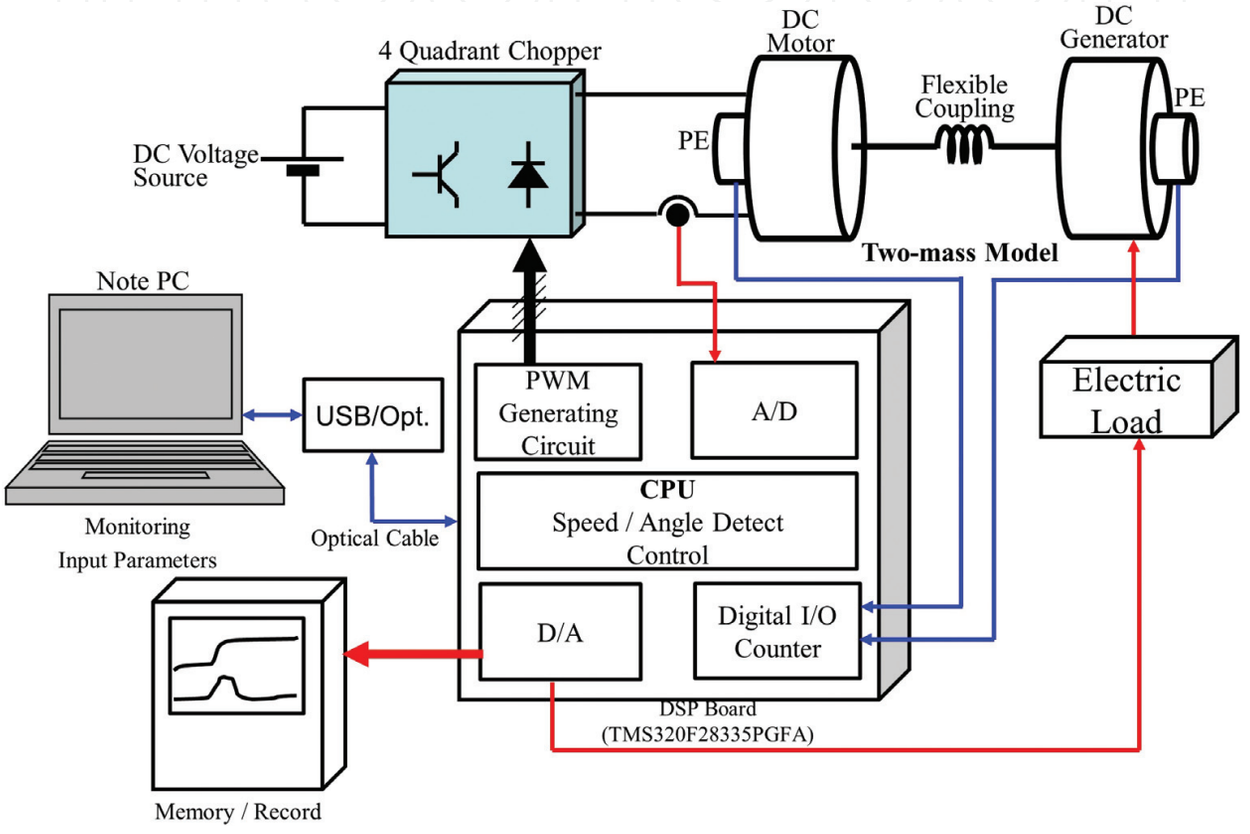

Figure 5. Configuration of the experimental system (for the two-mass resonance model).

2.2. Modified-IPD speed controller and PI current controller

In this chapter, classical PID speed and current controllers are used to suppress the resonance vibrations for the two-mass resonance model. In general, the PI controller, which consists of a proportional controller and an integral controller that are placed in parallel to determine the speed error, is used as the angular speed controller. However, because the resonance system has a complex structure, it is difficult to suppress the vibrations using the classic PI controller alone. Therefore, the I-PD controller is used in this chapter and a first-order lag element is also used to increase the degrees of freedom for the controller design. Additionally, a simple PI controller is

used to realize the high-speed torque response for the current minor loop. The continuous control system proposed here is shown in **Figure 6**. In the figure, ω_{ref} is the reference angular speed, K_p, K_i, K_d, and T_d represent the m-IPD speed controller gains, and K_{ap} and K_{ai} are the PI current controller gains. This chapter proposes two design methods for these six controller gains (i.e., K_p, K_i, K_d, T_d, K_{ap}, and K_{ai}). Then, during the simulations and experiments, a digital control system is used, as shown in **Figure 7**. In this case, the D-control element of the speed controller performs a z-transform in combination with the first lag element of the speed controller to construct a difference equation and avoid the need for a complete differentiation procedure.

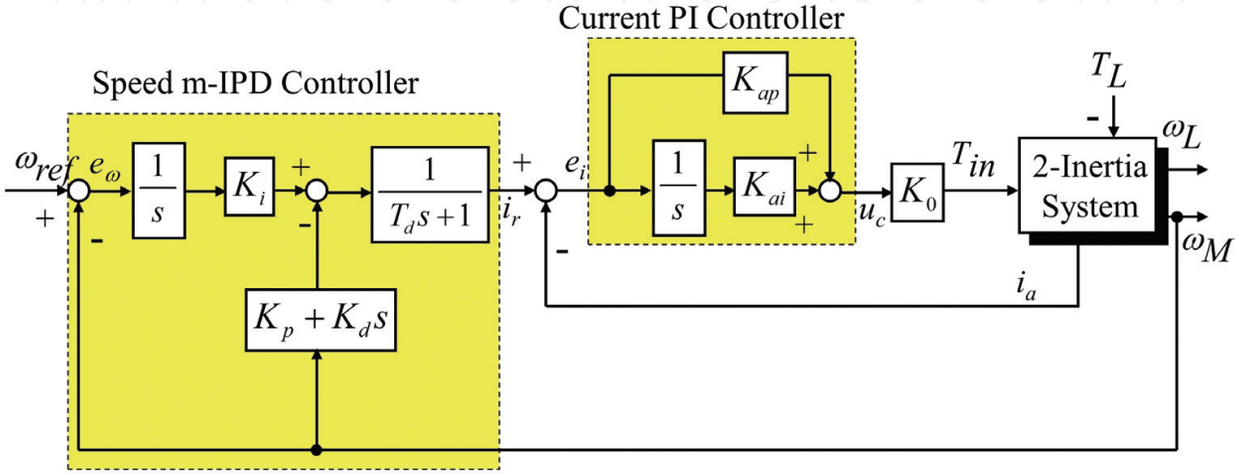

Figure 6. Proposed control system (continuous controller model).

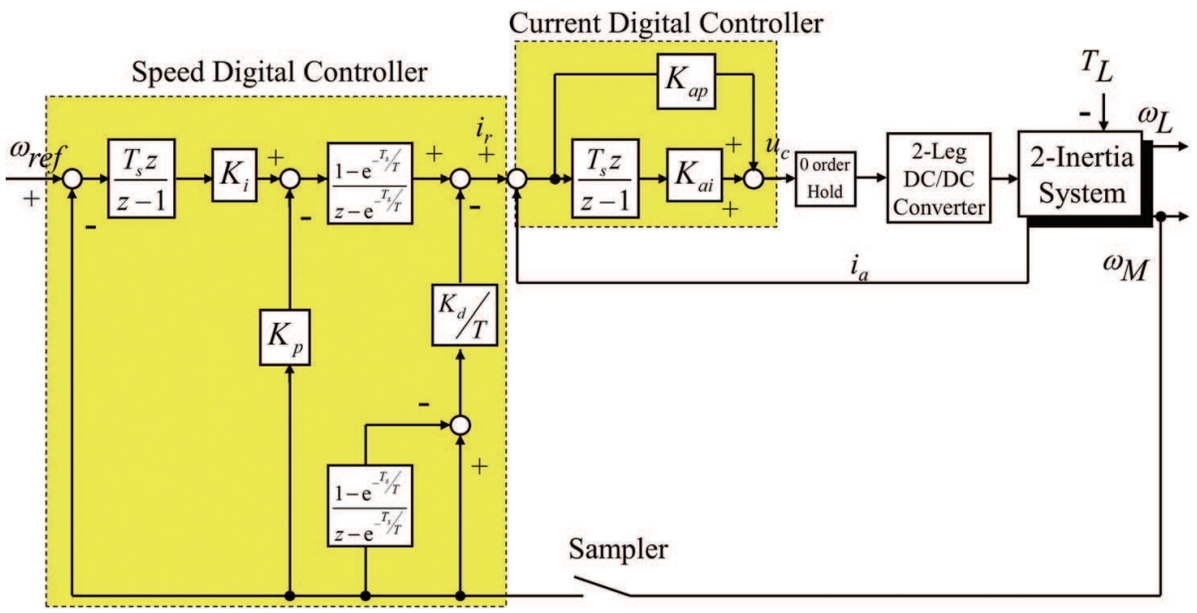

Figure 7. Proposed control system (discrete controller model).

3. Controller design using coefficient diagram method

3.1. Coefficient diagram method

First, this section explains the coefficient diagram method (CDM) for design of the proposed controller, which is required to suppress the resonance vibrations for the two-mass resonance model. The CDM is an algebraic approach that is used to design the characteristic polynomial directly in the parameter space. In the CDM, a coefficient diagram (CD) is used to perform the controller design. The CD provides the ability to analyze the time response, stability and robustness qualities of the controller using a diagram. In the CD, the vertical axis shows the coefficient of the characteristic polynomial (a_i), the stability indices (γ_i), and the equivalent time constant (τ) logarithmically, while the horizontal axis shows the order i values that correspond to the coefficient. Here, the characteristic polynomial is as shown in Eq. (12).

$$P(s) = a_n s^n + a_{n-1} s^{n-1} + \cdots + a_1 s + a_0 = \sum_{i=0}^{n} a_i s^i \tag{12}$$

In the CDM, the stability indices (γ_i), which are defined in Eq. (13) below, are indicators of the stability of the control system.

$$\gamma_i = \frac{a_i^2}{a_{i+1} a_{i-1}}, \qquad i = 1\tilde{n} - 1 \tag{13}$$

The equivalent time constant τ, which represents the transient response characteristic, is expressed using the following equation:

$$\tau = \frac{a_1}{a_0} \tag{14}$$

The coefficient a_i can then be calculated using τ and the stability indices γ_i as shown in Eq. (15).

$$a_{i+1} = \frac{a_0 \tau^i}{\gamma_{i-1} \gamma_{i-2}^2 \cdots \gamma_2^{i-2} \gamma_1^{i-1}} \tag{15}$$

In the CDM, use of the standard values of the stability indices is recommended, and these values are listed as follows:

$$\gamma_{n-1} = \cdots = \gamma_3 = \gamma_2 = 2.0, \qquad \gamma_1 = 2.5 \tag{16}$$

This form is called "the standard form of the stability indices."

3.2. Design method for the controller gains using the CDM

The CDM is a very simple and effective method for controller design. However, in higher order systems, it is difficult to complete the design by trial and error alone. In this work, the

http://dx.doi.org/10.5772/intechopen.74298

design of the CD for the control system is performed using the differential evolution (DE) method. The DE method is an optimization search method [12, 13].

In the proposed design method, the reference value of the equivalent time constant τ_{ref} is first specified. Then, the coefficients of the characteristic polynomial are calculated using the six controller gains with random initial settings. Each of the coefficients is determined using the following equations:

$$a_7 = J_{Mpu} T \tau_e \tag{17}$$

$$a_6 = J_{Mpu} \tau_e + J_{Mpu} T + J_{Mpu} K_{ap} T \tag{18}$$

$$a_5 = J_{Mpu} + J_{Mpu} K_{ap} + K_{ap} K_d + K_{epu} T + J_{Mpu} K_{ai} T + J_{Mpu} T \tau_e \omega_r^2 \tag{19}$$

$$a_4 = K_{epu} + J_{Mpu} K_{ai} + K_{ai} K_d + K_{ap} K_p + J_{Mpu} T \omega_r^2 + J_{Mpu} \tau_e \omega_r^2 + J_{Mpu} K_{ap} T \omega_r^2 \tag{20}$$

$$a_3 = J_{Mpu} \omega_r^2 + K_{ap} K_i + K_{ai} K_p + J_{Mpu} K_{ap} \omega_r^2 + K_{ap} K_d \omega_a^2 + K_{epu} T \omega_a^2 + J_{Mpu} K_{ai} T \omega_r^2 \tag{21}$$

$$a_2 = K_{epu} \omega_a^2 + K_{ai} K_i + J_{Mpu} K_{ai} \omega_r^2 + K_{ai} K_d \omega_a^2 + K_{ap} K_p \omega_a^2 \tag{22}$$

$$a_1 = K_{ap} K_i \omega_a^2 + K_{ai} K_p \omega_a^2 \tag{23}$$

$$a_0 = K_{ai} K_i \omega_a^2 \tag{24}$$

The stability indices are then computed using these calculated coefficients and the evaluation function F in Eq. (25) is calculated using the terms from Eqs. (26)–(30). In this case, the evaluation function F consists of an evaluation to match with the set reference value of the equivalent time constant, an evaluation to reduce the change in the next stability index, and an evaluation to match the standard forms of the stability indices $\gamma_{s,i}$. The weights w_1 to w_5 of the evaluation functions are set to have values of (w_1, w_2, w_3, w_4, w_5) = (100, 2, 10, 1, 4), respectively. These steps are subsequently repeated to obtain the optimal controller gains by the DE method.

$$F = \frac{1}{w_1 f_1 + w_1 f_1 + w_1 f_1 + w_1 f_1 + w_1 f_1} \tag{25}$$

$$f_1 = \sqrt{(\tau_{ref} - \tau)^2} \tag{26}$$

$$f_2 = \sum_{i=1}^{2} \sqrt{\left(\gamma_{s,i} - \gamma_i\right)^2} \tag{27}$$

$$f_3 = \sqrt{\left(\gamma_{s,3} - \gamma_3\right)^2} \tag{28}$$

$$f_4 = \sum_{i=3}^{5} \sqrt{(\gamma_i - \gamma_{i+1})^2} \tag{29}$$

$$f_5 = \sum_{i=4}^{6} \sqrt{\left(\gamma_{s,i} - \gamma_i\right)^2} \tag{30}$$

3.3. Simulation results

Figure 8 shows an example of the simulation results in the form of the angular speed step responses for the control input. The resonance vibrations can be seen in this figure.

Figure 9 shows the frequency response characteristics of the two-mass resonance model from the control input u_c to the motor angular speed ω_M. The peak point of the mechanical resonance can be observed in this figure. It is therefore essential to construct the controller design method such that it reduces this resonance peak gain.

Table 2 shows the controller gains that were designed using the proposed method, where the reference time constant τ_{ref} is set to 0.05. **Figure 10** shows the designed CD. In the figure, each coefficient is multiplied by 100^n, where n is the order of the characteristic polynomial. The figure shows that the form of the diagram is very smooth and that the convex shape is appropriately upward. The designed stability indices are shown in **Figure 11**. The results in this figure confirm that the stability indices nearly fit the standard form of these indices, and the fluctuations in the numerical values of adjacent indices are also small.

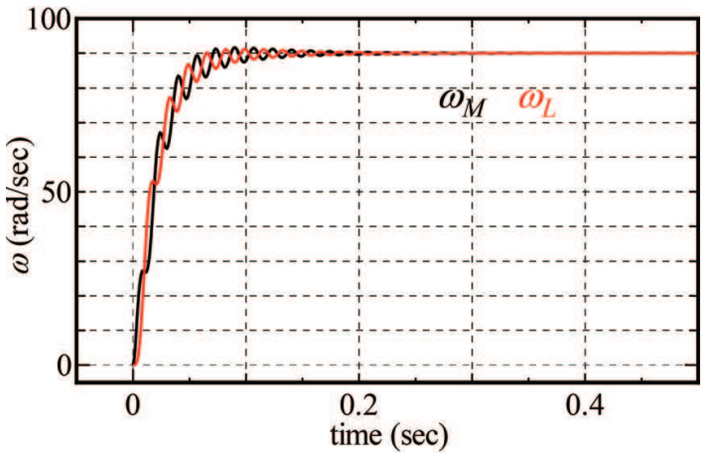

Figure 8. Angular speeds of the step responses of the two-mass model.

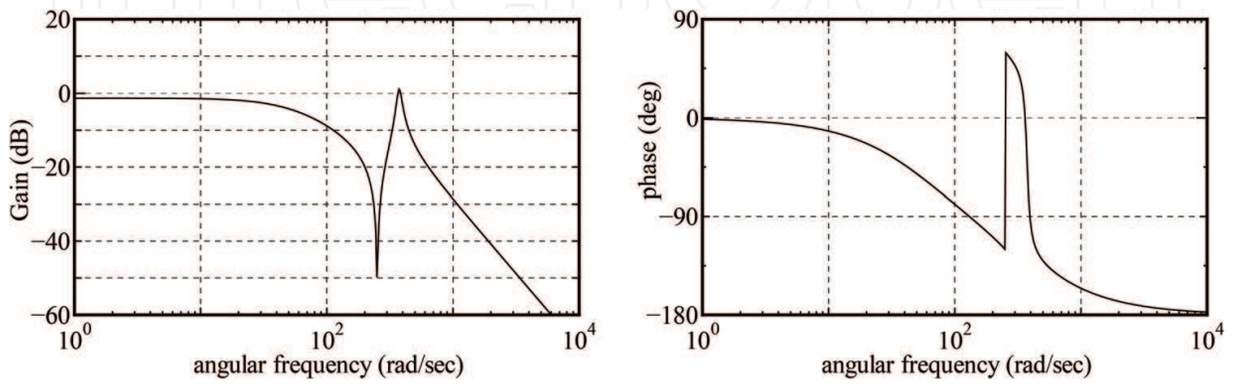

Figure 9. Frequency responses of the two-mass resonance model from u_c to ω_M.

http://dx.doi.org/10.5772/intechopen.74298

Gain name	Value	Gain name	Value	Gain name	Value
K_p	2.792×10^2	K_i	9.007×10^3	K_d	3.522
T	0.4368	K_{ap}	1.834	K_{ai}	96.53

Table 2. Controller gain results when designed using the proposed CDM method.

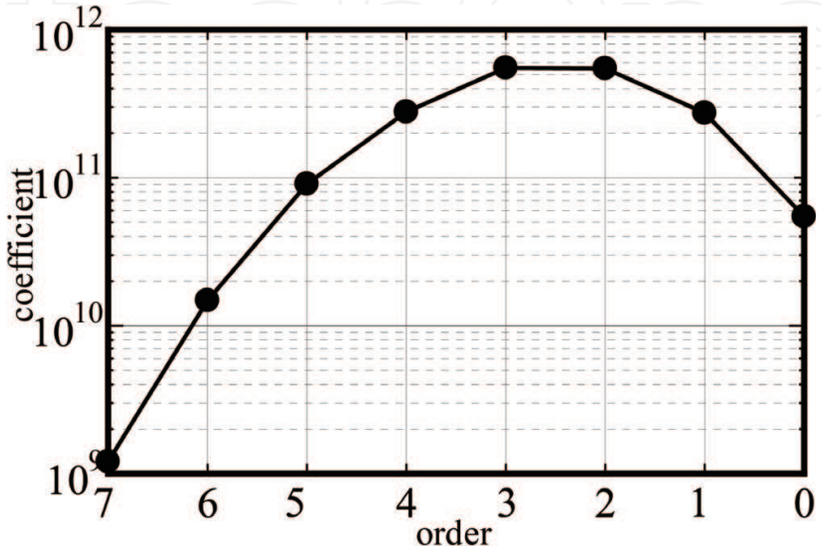

Figure 10. Designed coefficient diagram.

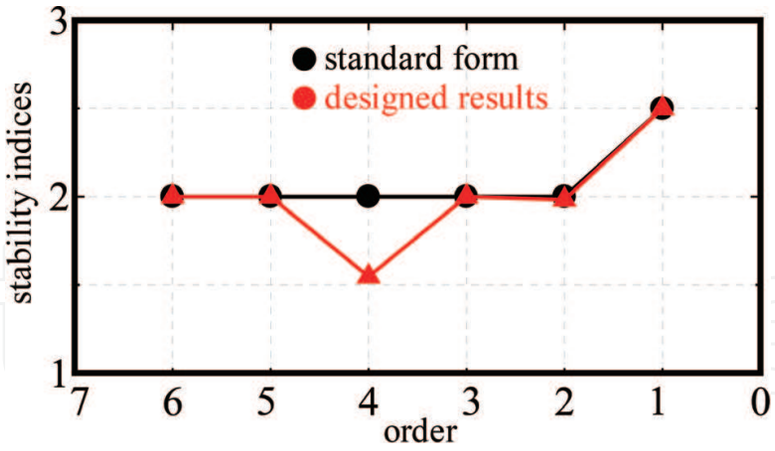

Figure 11. Designed and standard form stability indices.

Figure 12 shows the simulation results, where the speed reference command input ω_{ref} is changed from 0 to 30 rad/s at t = 0 s, and the disturbance torque input is changed from 0 to 20% of the rated torque at t = 0.25 s. The figure indicates that the wave provides a good reference-following performance and illustrates the validity of the vibration suppression characteristics and the disturbance response simultaneously. Additionally, the gain characteristic that was derived using the proposed method over the range from the reference speed ω_{ref} to

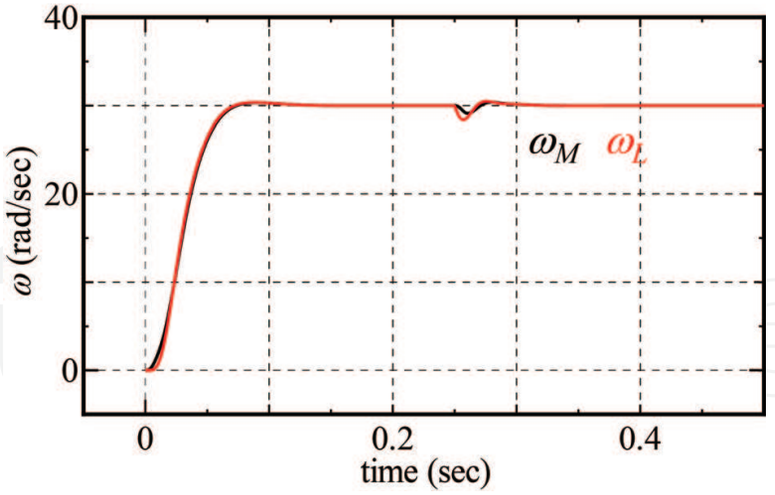

Figure 12. Simulation results when using the proposed method.

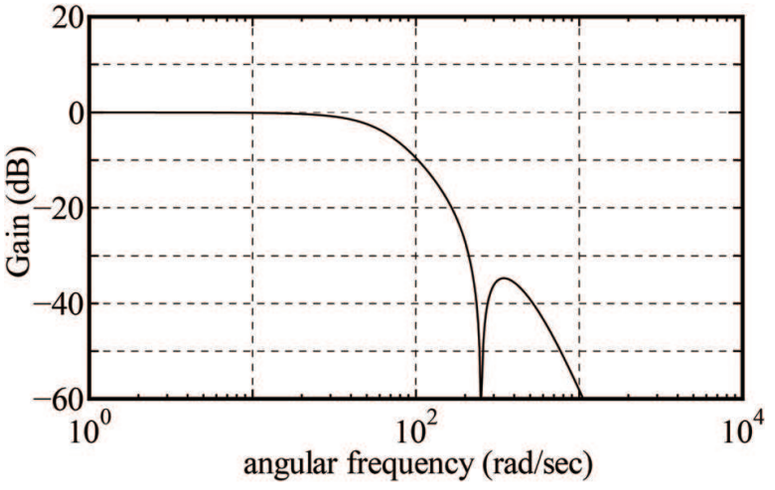

Figure 13. Gain characteristics when using the proposed method over the range from ω_{ref} to ω_M.

the motor angular speed ω_M is illustrated in **Figure 13**. The effectiveness of the proposed method is confirmed by the characteristic shown in this figure because the resonance peak is reduced considerably. Therefore, the results for the proposed method show that it is effective as a design method for the vibration suppression controller for the two-mass resonance system.

4. Controller design using fictitious reference iterative tuning (FRIT)

In this section, an off-line tuning method for the vibration suppression-type speed and current controller gains for the two-mass system is proposed based on the FRIT method; this method uses only single-shot experimental input-output data and does not use either the model parameters or the state equation of the two-mass resonance model. While most FRIT designs only use one state variable, this method uses specific multiple state variables to design the controller gains when using the FRIT method [6, 7, 14–16].

4.1. Frit

Figure 14 shows a typical control system, in which G is the transfer function of the object to be controlled, r is the reference signal, $\boldsymbol{\rho}$ represents the controller gains, $C(\boldsymbol{\rho})$ represents the controller, u is the control input parameter, and y is the output parameter. In this case, the mathematical model of G is not known in advance and is not required for this method.

Initially, as shown in **Figure 15**, a single-shot experiment is performed using the initial controller gains ρ_0, and the control input u_0 and output y_0 are measured. Then, the reference model $M(s)$, which matches the desired response, is determined. A fictitious reference signal is then generated using the controller, the control input u_0, and the output y_0, as shown in Eq. (31) below. This means that the initial data u_0 and y_0 can be obtained using any value of ρ if $\tilde{r}(\boldsymbol{\rho})$ is input to the closed-loop system used to implement $C(\boldsymbol{\rho})$.

$$\tilde{r}(\boldsymbol{\rho}) = C(\boldsymbol{\rho})^{-1}u_0 + y_0 \tag{31}$$

The optimal controller gains that are required to achieve $y_M = y_0$ are then determined, as shown in **Figure 16**, using an optimization search method. Finally, these controller gains then represent the best available solutions that allow the desired control system response to be obtained. Therefore, the controller design process can be performed without any prior information about either the model parameters or the state equations.

4.2. Vibration suppression controller design method by FRIT

Figure 17 shows a simplified form of the proposed vibration suppression control system, where $C_{\omega 1}$, $C_{\omega 2}$, $C_{\omega 3}$, and C_i are the controllers. While the FRIT method generally uses one

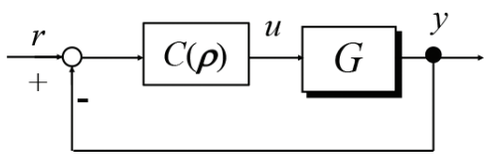

Figure 14. Typical closed-loop system.

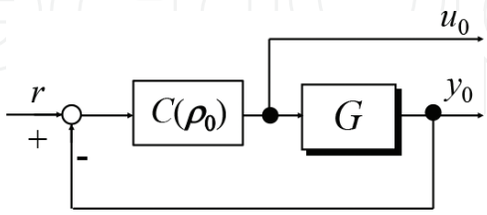

Figure 15. Measurement of the initial data.

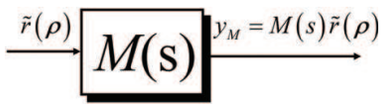

Figure 16. Reference model showing the input of the fictitious reference signal.

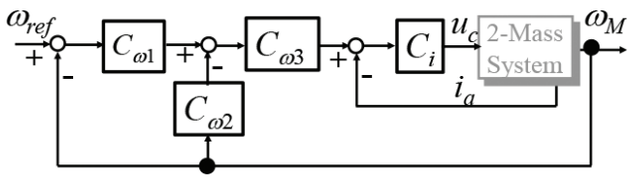

Figure 17. Simplified proposed control system.

control input and one state variable for the initial experimental data, the proposed method uses one control input, u_c, plus two state variables, ω_M and i_a. The controller gain vector $\boldsymbol{\rho}$ is given as follows:

$$\boldsymbol{\rho} = \begin{bmatrix} K_p & K_i & K_d & TK_{ap} & K_{ai} \end{bmatrix}^T \tag{32}$$

Therefore, the fictitious reference signal $\tilde{\omega}_{ref}(\boldsymbol{\rho})$ can be calculated using the following equation without any need for the two-mass resonance model.

$$\tilde{\omega}_{ref}(\boldsymbol{\rho}) = \left(1 + C_{\omega 1}^{-1} C_{\omega 2}\right)\omega_{M0} + C_{\omega 1}^{-1} C_{\omega 3}^{-1} i_{a0} + C_{\omega 1}^{-1} C_{\omega 3}^{-1} C_i^{-1} u_{c0} \tag{33}$$

Here, u_{c0}, ω_{M0} and i_{a0} represent the initial experimental data. The reference model $M(s)$, as shown in Eq. (34), is then used depending on the purpose of the system, where the time constant τ is a reference model parameter.

$$M(s) = \frac{1}{(\tau s + 1)^3} \tag{34}$$

Here, τ is calculated using the following equation with the 99% response time parameter T_{99}.

$$\tau = \frac{T_{99}}{4.4 \times 3^{0.6}} \tag{35}$$

The differential evolution method is then used to search for the optimal gains. The performance index function F is then defined as shown in Eq. (36) below using ω_{M0} and $y_M = M(s)\tilde{\omega}_{ref}(\boldsymbol{\rho})$.

$$F(\boldsymbol{\rho}) = \left\| M(s)\tilde{\omega}_{ref}(\boldsymbol{\rho}) - \omega_{M0} \right\|_2 \tag{36}$$

4.3. Experimental results

Figure 18 shows an example of the experimental results in the form of the angular speed step response of the control input. The resonance vibrations can again be observed in a similar manner to the case of the simulation results shown in **Figure 8** above.

Figure 19 shows the gain characteristics of the frequency responses from the experimental results shown in **Figure 18**, which relate the input voltage to the motor angular speed ω_M and the load angular speed ω_L. From these characteristics, the peak resonance vibrations at approximately 300 rad/s are also observed. These results were calculated based on the experimental

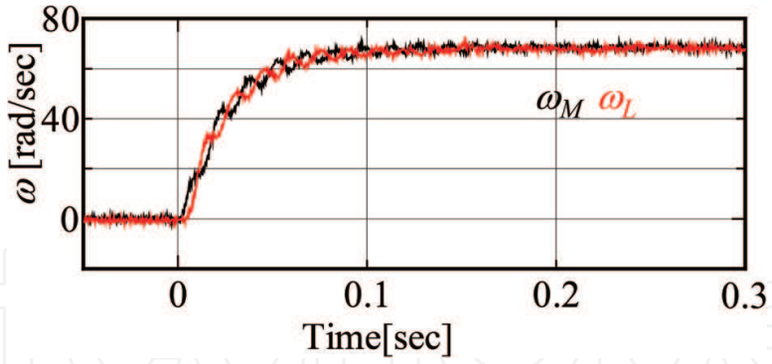

Figure 18. Angular speeds of the step responses (DC voltage input).

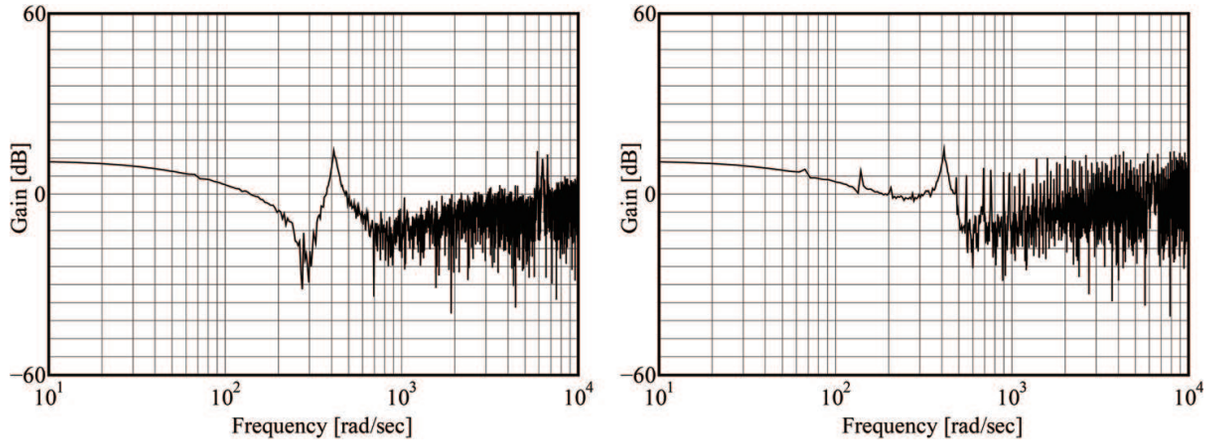

Figure 19. Calculated frequency responses to dc voltage input (left: u_c to ω_M, right: u_c to ω_L).

input and output waves of the voltage step response using the method that was proposed in [20]. Additionally, both the resonance and anti-resonance points can be found in these figures.

Figure 20 shows the experimental results obtained when using the general PI speed and current controller for comparison with the effects of the proposed control system. **Figure 21** shows the gain characteristics for the frequency responses shown in **Figure 20**, which relate ω_{ref} to ω_M and ω_L, where ω_{ref} is 30 rad/s. These characteristics show that the peak gain of the

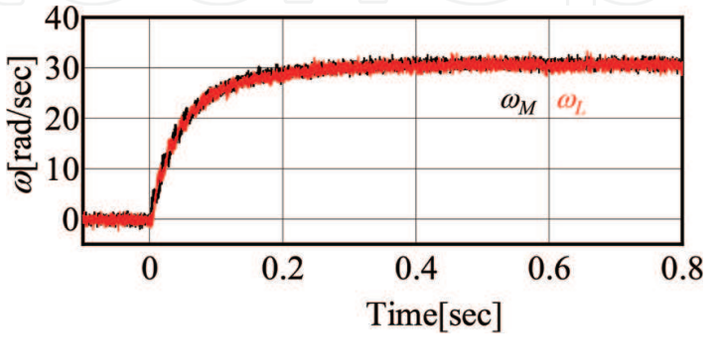

Figure 20. Experimental results obtained using conventional PI controller.

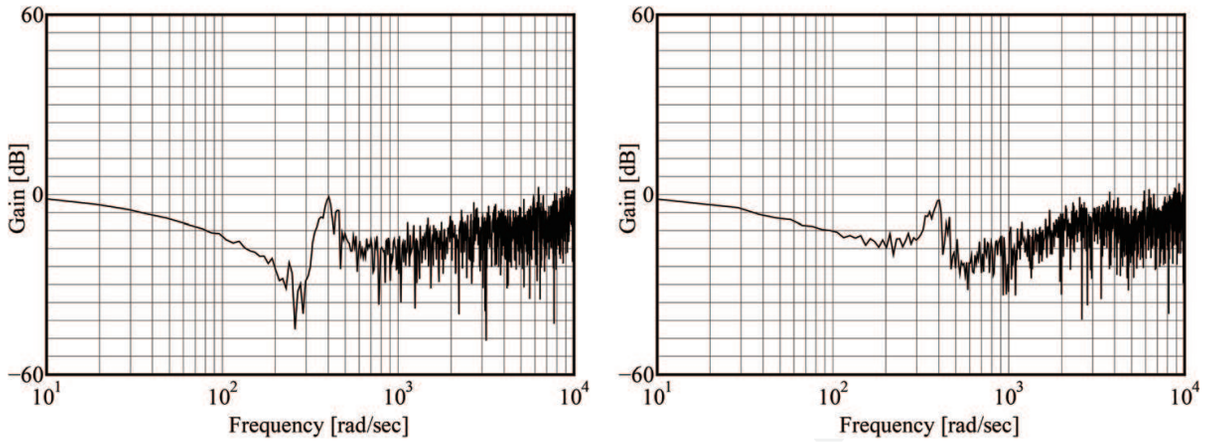

Figure 21. Frequency responses of conventional PI speed control system (left: ω_{ref} to ω_M; right: ω_{ref} to ω_L).

resonance is not greatly attenuated. **Figures 22–24** show the initial experimental waves for ω_{M0}, i_{a0} and u_{c0}, respectively, that were obtained using the values of the initial controller gain ρ_0, which are listed as follows:

$$\boldsymbol{\rho}_0 = [\,0.1 \quad 30 \quad 0.0001 \quad 0.001 \quad 1 \quad 10\,]^T \tag{37}$$

Both the initial rise and the oscillation can be observed in these figures.

Table 3 shows the results for the controller gains determined using the proposed FRIT design method with searching by the DE method, where T_{99} was set at 0.2 s. **Figure 25** shows a comparison of the experimental results obtained using the controller gains that were designed using the proposed method with the simulated results for the reference output y_M. The results in the figure show that the proposed off-line tuning method works very well, despite the fact that the design was performed using the initial one-shot experimental data alone. **Figure 26**

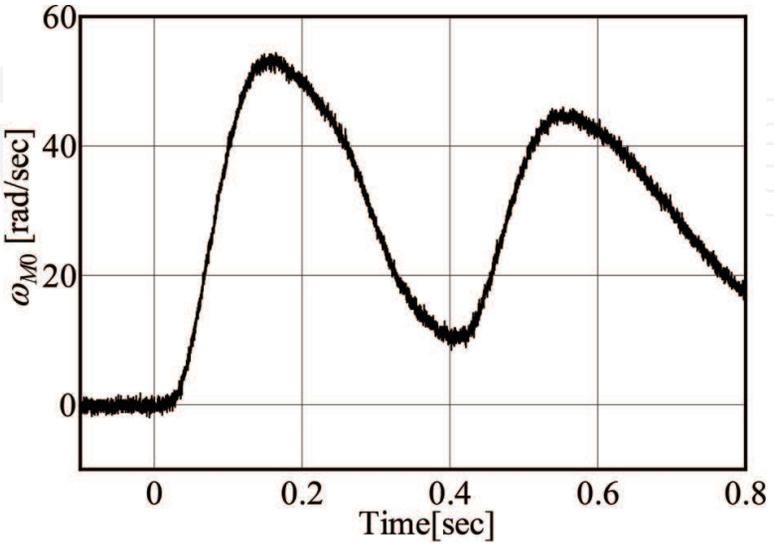

Figure 22. Initial ω_{M0} data.

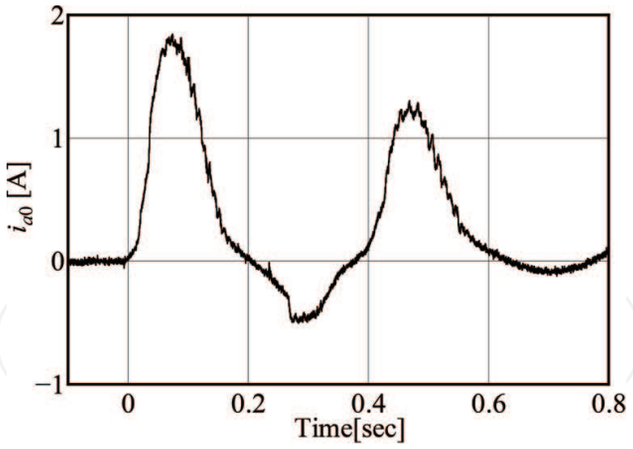

Figure 23. Initial i_{a0} data.

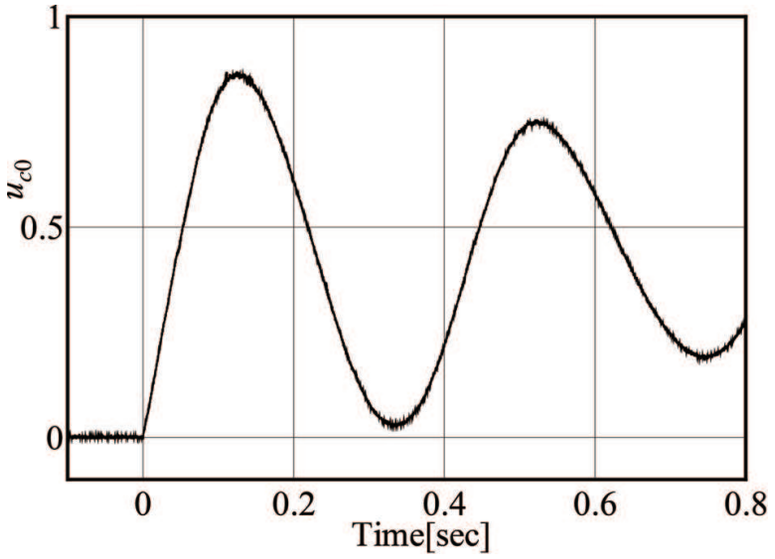

Figure 24. Initial u_{c0} data.

Gain name	Value	Gain name	Value	Gain name	Value
K_p	1.24	K_i	17.0	K_d	6.53×10^{-3}
T	8.59×10^{-4}	K_{ap}	2.37	K_{ai}	135

Table 3. Controller gain results when designed using the proposed FRIT method.

shows the experimental results that were obtained for ω_M, ω_L, and i_a when the proposed FRIT method was used. Here, ω_{ref} is stepped from 0 to 30 rad/s when t is 0 s. The figure shows the good response of the proposed vibration suppression speed controller. **Figure 27** shows the experimental results, where ω_{ref} is stepped from 30 to 50 rad/s when t is 0 s and the disturbance torque is increased from 0 to 10% of the rated torque when t is 0.5 s. As these figures show, good waves were observed in terms of their reference-following performance and disturbance response.

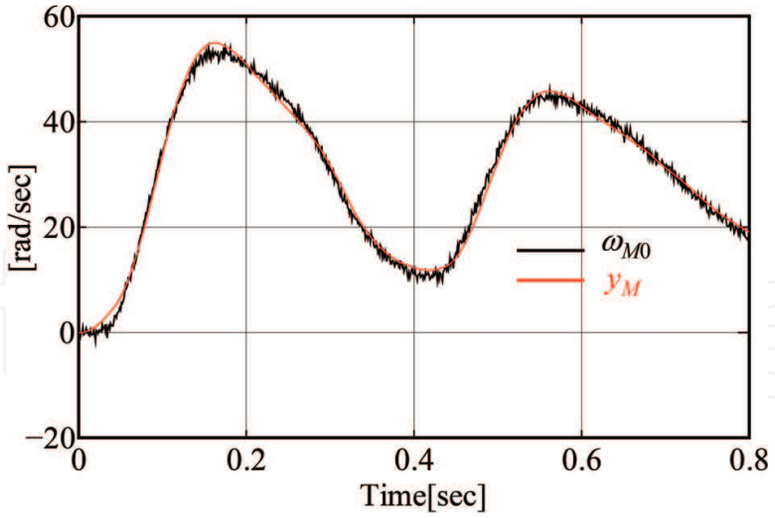

Figure 25. Initial experimental results for ω_{M0} and simulation results for y_M.

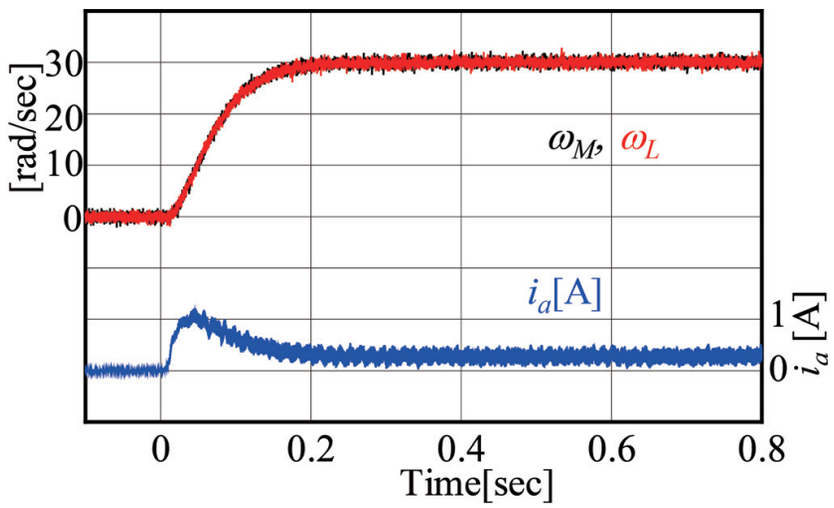

Figure 26. Experimental results for ω_M, ω_L, and i_a obtained when the proposed FRIT method.

Figure 28 shows the gain characteristics of the frequency responses of the proposed control system, where these characteristics are shown from the perspectives of ω_{ref} relative to ω_M and ω_L. The resonance vibration suppression effect can be observed in these figures. Therefore, the effectiveness of the proposed control system and the design method based on use of the FRIT method can be confirmed. Additionally, **Figure 29** shows the experimental results (ω_L) that were obtained for various values of the speed reference time parameter, where T_{99} = 0.15, 0.175, 0.2, 0.25, 0.3, and 0.35. As shown in this figure, the response times change satisfactorily and the proposed design method for the controller gains can thus also be used to design the response times arbitrarily.

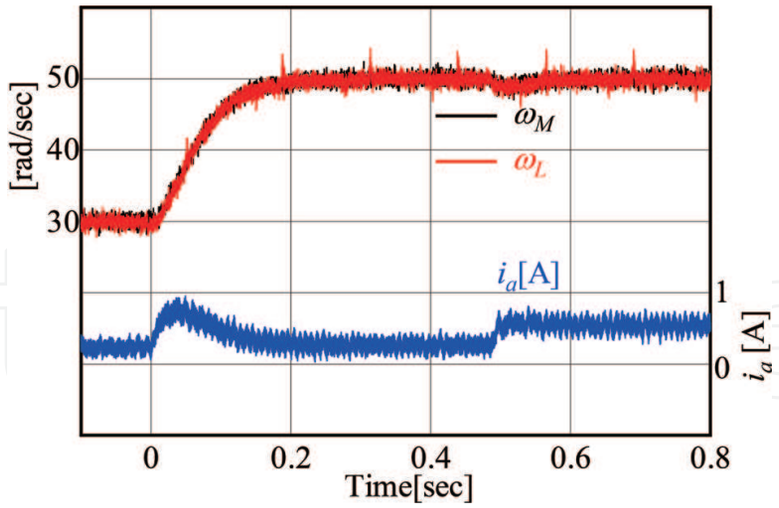

Figure 27. Experimental results for speed step response and disturbance response.

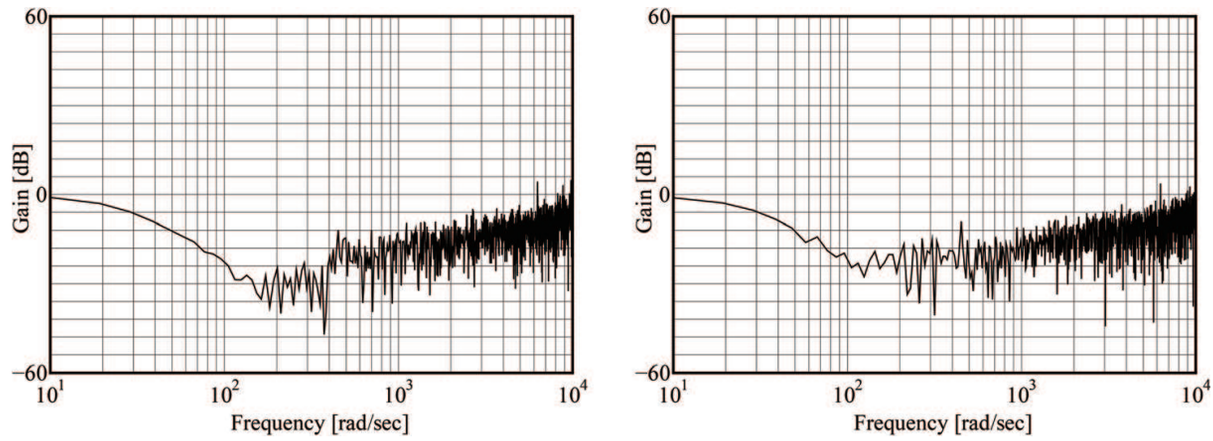

Figure 28. Frequency responses of the proposed control system (left: ω_{ref} to ω_M; right: ω_{ref} to ω_L).

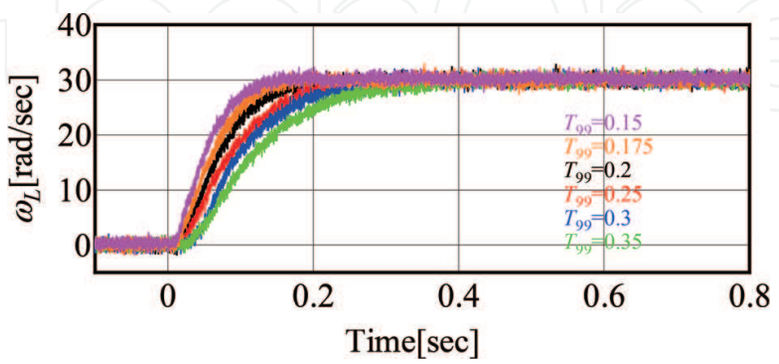

Figure 29. Experimental responses of ω_L to various values of T_{99}.

5. Conclusion

This chapter has proposed two design methods for the controller gains required for vibration suppression control in a two-mass resonance system. The proposed controller consists of a modified-IPD speed controller and a PI current controller. The proposed controller design methods are based on application of the coefficient diagram method (CDM) and application of the fictitious reference iterative tuning (FRIT) method. Both methods use the motor side variables only, including the motor's angular speed and the armature current. The CDM method uses the coefficient of the characteristic polynomial of the control system and can determine the control performance based on the shape of the coefficient diagram and the stability indices. In this chapter, the fitting performances for the standard form of the stability indices and the coefficient values were used to determine the controller gains, which were designed using the differential evolution method. The effectiveness of the proposed CDM was confirmed by the simulation results. The FRIT method can be used to design the controller without knowledge of the model state equations and their parameters. Furthermore, a fictitious signal that was calculated using the initial experimental data for multi-state variables was also proposed in this chapter. The effectiveness of the proposed FRIT method was confirmed using the experimental results. Consequently, the CDM and the FRIT method were shown to produce the same design performance. The CDM is useful for controller design when the mathematical model and the object parameters are known. The FRIT method is effective when the mathematical model is unknown but the initial experimental data can be observed.

Author details

Hidehiro Ikeda

Address all correspondence to: ikeda@nishitech.ac.jp

Department of Electrical Engineering, Nishi-Nippon Institute of Technology, Japan

References

[1] Hori Y, Sawada H, Chun Y. Slow resonance ratio control for vibration suppression and disturbance rejection in torsional system. IEEE Transactions on Industrial Electronics. 1999;**46**(1):162-168

[2] Yoon K-H et al. Hybrid robust controller design for a two mass system with disturbance compensation. Proceedings of ICCAS 2008; **2008**:1367-1372

[3] Ikeda H, Hanamoto T, Tsuji T, Tanaka Y. Position control of 2-mass systems with speed minor loop designed by pole placement method. IEEJ Transactions on Industry Applications. 1999;**119-D**(4):544-545 (in Japanese)

[4] Ikeda H, Hanamoto T, Tsuji T. Design of multi-inertia digital speed control system using Taguchi method. Proc. of ICEM 2008; 2008. pp. 1-6. Paper ID 1167, PB.3.9

[5] Ikeda H, Hanamoto T, Tsuji T, Tomizuka M. Design of vibration suppression controller for 3-inertia systems using Taguchi method. Proc. of SPEEDAM 2006, Mechatronic Systems; 2006. pp. S10–19-S10–25

[6] Matsui Y, Ayano H, Nakano K. A controller tuning for 2-mass system using closed-loop transient data, Proc. of 11th IFAC International Workshop, THS6T2. 1; 2013. pp. 564-569

[7] Azuma T, Watanabe S. A design of PID controllers using FRIT-PSO. Proc. of 8th ICST; 2014. pp. 459-464

[8] Manabe S, Kim Y-C. Recent development of coefficient diagram method. Proc. of 3rd Asian Control Conference; 2000. pp. 2055-2060

[9] Hanamoto T, Takenouchi T, Ikeda H. Vibration suppression control of 3-mass resonance system using particle swarm optimization for Design of Coefficient Diagram Method. Journal of Japan AEM. 2011:S16-S20

[10] H. Ikeda, T. Hanamoto. Vibration suppression control for multi-mass system using CDM designed by group-based-PSO. Proc of ICEE 2012, P-EM-12; 2012. pp. 1160-1165

[11] Ikeda H, Hanamoto T. Fuzzy controller of three-inertia resonance system designed by differential evolution. Journal of International Conference on Electrical Machines and Systems. 2014:184-189

[12] Ikeda H, Hanamoto T. Fuzzy controller of multi-inertia resonance system designed by differential evolution. Proc of ICEMS 2013, MC-1883; 2013. pp. 2291-2295

[13] Ikeda H, Hanamoto T. Design of m-IPD controller of multi-inertia system using differential evolution. Proc of IPEC 2014, 21J1–2; 2014. pp. 2476-2482

[14] Ikeda H, Hanamoto T. Design of vibration suppression controller for 2-inertia system by fictitious reference iterative tuning. Proc of ICEE 2015, ICEE15A-123; 2015. p. 6

[15] Ikeda H, Ajishi H, Hanamoto T. Application of fictitious reference iterative tuning to vibration suppression controller for 2-inertia resonance system. Proc of IECON 2015, TS-48, YF-008451. 2015. pp. 1825-1830

[16] Ikeda H, Kogura Y, Kim K, Era R, Hanamoto T. Vibration suppression controller tuning method for 2-mass resonance system using FRIT, Proc of ICEMS 2016, DS4G-3-2; 2016. p. 6

[17] Ikeda H. Vibration Suppression Controller of Multi-Mass Resonance System Using Fuzzy Controller. In: Chapter 19 of Modern Fuzzy Control Systems and Its Applications. Rijeka: InTech; 2017. pp. 399-417. ISBN 978-953-51-3390-2

[18] Myway Plus Corporation, https://www.mayway.co.jp/, Yokohama, Japan

[19] The Mathworks, https://www.mathworks.com, Massachusetts, U.S.A

[20] Matsui Y, Kimura T, Nakao K. Frequency response estimation for mechanical systems using closed-loop step response data. IEEJ Transactions on Electronics, Information and Systems. 2011;**131**(5):751-757

IntechOpen